Implementation of compressed sensing method for foot pressure reconstruction based on AI

Viet Nguyen Van[1], Duc Nguyen Dinh[2], Thang Nguyen Huu[3], Hoang Anh Pham[4], Hoai Nam Vu[5], Van-Thuc Tran[2], Tin Nguy Phan[1*]

[1] School of Engineering Physics, Hanoi University of Science and Technology, Hanoi, Vietnam
{viet.nv1305}@outlook.com, {tin.nguyphan}@hust.edu.vn

[2] School of Mechanical Engineering, Hanoi University of Science and Technology, Hanoi, Vietnam
{ddinhf.dduwcs}@gmail.com, {thuc.tranvan}@hust.edu.vn

[3] Sun Group International Hospital Hanoi, Vietnam
{nguyenhuuthang.fet}@gmail.com

[4]Autonomous Vehicles and Intelligent Systems Laboratory, [5]Young Innovation Research Laboratory on Digital Technology, Posts and Telecommunications Institute of Technology, Hanoi, Vietnam
{anhph, namvh}@ptit.edu.vn

***Abstract*—The quality of life is significantly affected by abnormalities in gait brought on by diseases like flat feet, Parkinson's disease, or stroke. This work presents the development of a plantar pressure monitoring system that utilizes gait analysis to aid in clinical evaluation and rehabilitation. The technology records pressure data in real-time at key plantar areas using eight Force Sensitive Resistor (FSR) sensors inserted in a mat. Reconstructing high-resolution plantar pressure maps from a small number of sensor inputs is made possible by an innovative use of compressed sensing (CS). For accurate signal reconstruction, the system employs a K-SVD–based dictionary learning framework combined with Orthogonal Matching Pursuit (OMP), where the pressure map is modeled as a sparse signal in a learned representation domain. Experimental results using a public dataset and real measurements demonstrate that the reconstructed images closely match ground truth data, with a Pearson correlation of 95.65%. This proves the feasibility of reconstructing detailed pressure distributions from sparse input data.**

***Index Terms*—FSR; pressured mat; smart insole; compressed sensing.**

I. Introduction

Daily mobility and physical activity are essential human needs. However, many people experience difficulties in movement due to congenital conditions (such as flat feet), Parkinson's disease, or post-stroke sequelae. These problems often result in gait imbalances, negatively impacting mobility and overall quality of life. Consequently, recent studies [1]–[3] have focused on developing systems to assist in the diagnosis and treatment of motor disorders. An widely adopted approach involves analyzing the distribution of plantar pressure during movement [4]. However, most current sensing systems are limited to monitoring contact forces and do not adequately assess or predict movement patterns in individuals with disabilities. Therefore, the development of a plantar pressure measurement system integrated with gait analysis to support rehabilitation is both necessary and timely. In this study, the authors employ Force Sensitive Resistor (FSR) sensors due to their advantages of being thin, lightweight, and easily integrable into mats or shoe insoles. FSR sensors generate voltage signals that vary with the applied force, making them suitable for electronic signal processing. However, given the small magnitude and susceptibility to noise of these signals, the research focuses on optimizing sensor configuration, signal amplification, and noise filtering. The acquired data are then fed into an artificial intelligence (AI) model to reconstruct and predict plantar pressure maps. This system facilitates gait assessment by comparing with normative patterns and suggesting interventions to improve mobility in people with disabilities. To prove the concept and prototype system, the authors focus on the reconstruction of static foot pressure based on the Compressed Sensing method.

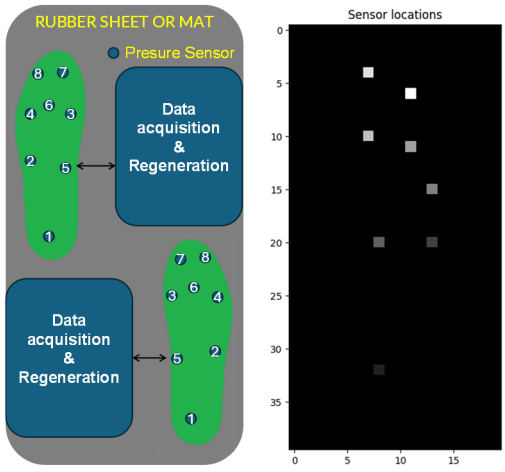

Fig. 1. System Overview of the Plantar Pressure Measurement System and Eight sensor locations as pixels of image.

II. Proposed Data Acquisition and Regeneration Techniques

According to recent studies [5] a typical plantar pressure measurement system comprises three main components, as illustrated in Fig. 1. Pressure sensors can be implemented

* Corresponding author

using various technologies such as resistive, capacitive, or piezoelectric sensors [6], [7]. They are strategically placed on the insole or a rubber mat to capture pressure data at key contact points during movement. (II) Data acquisition and processing unit includes electronic components such as analog–to–digital converters (ADC), a micro-controller (MCU), and communication modules. The analog signals from the pressure sensors are converted into digital form for further processing, storage, or transmission to the analysis system. (III) Data analysis or reconstruction system applies machine learning techniques, artificial neural networks (ANN), or other AI algorithms to analyze pressure patterns, reconstruct plantar pressure maps, and support clinical diagnosis or gait analysis.

A. FSR piezoresistive sensor

To enable real-time monitoring and analysis of gait parameters, the sensors must meet several requirements, including linearity, pressure range, and frequency response, and repeatability.

The FSR sensor (Fig. 2 (a-b) is a passive two-terminal device whose resistance changes – increases or decreases – when pressure is applied to the sensor sensitive area (SSA) [8], [9]. The SSA is typically composed of conductive particles randomly dispersed within a non-conductive polymer matrix. This layer is sandwiched between two metal electrodes, and the resulting change in resistance is measured. Materials commonly used in the fabrication of the SSA include elastomers, rubber, and polydimethylsiloxane (PDMS). The conductive particles can be derived from various metals, such as nickel or copper, with particle sizes ranging from tens of nanometers to several micrometers.

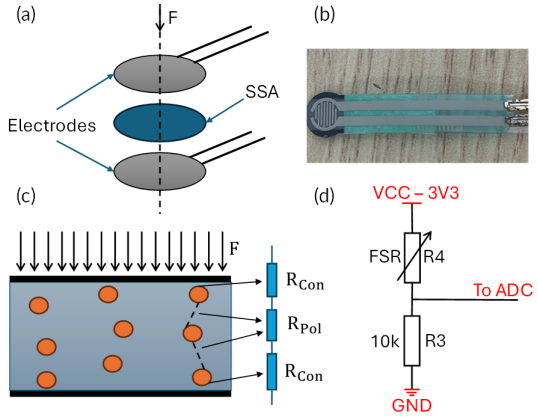

Fig. 2. (a) FSR piezoresistive sensor structure; (b) FSR piezoresistive sensor; (c) the equivalent electrical circuit model of a FSR; (d) The circuit schematic of the voltage divider configuration.

When a force is applied, the conductive particles within the SSA move closer together, resulting in a decrease in the sensor resistance (Fig. 2 (c-d)). At this point, the resistance of the FSR sensor can be determined using the following equation:

$$R_{\text{total}} = 2R_{\text{Con}} + R_{\text{Pol}} \tag{1}$$

$$V_{\text{out}} = \frac{V_{\text{cc}} \cdot R_{\text{FSR}}}{R_3 + R_{\text{FSR}}} \tag{2}$$

After minimizing the influence of power supply noise, a relationship between applied pressure and the electrical resistance characteristic of the sensor must be addressed because of variations in the number and distribution of conductive particles within the polymer layer of each sensor. Standard calibration weights were applied statically to the FSR sensors to generate a range of known pressure values.

B. Sensor array design and signal acquisition circuit

1) Sensor Placement: Accurately capturing the force distribution at various locations on the foot during movement is essential for monitoring individuals undergoing rehabilitation. Based on a review of recent studies [10], the authors identified eight key locations on the human foot for sensor placement (Fig. 1). Placing sensors at these critical locations allows for the collection of important data regarding plantar pressure distribution. This configuration is also applicable to individuals with flat feet. Therefore, the system is suitable for gait analysis and functional assessment in both normal and pathological cases.

2) Sensor data acquisition system: This section focuses on accurately measuring the resistance values of FSR sensors based on previously calibrated data. Each sample undergoes multiple measurements. After completing the sensor calibration, the authors designed a signal acquisition system using eight FSR sensors (Fig. 3) arranged on a mat to collect pressure data from various locations on the foot. The varying resistance signals from the FSR sensors are first fed into a signal conditioning unit, which performs voltage division, noise filtering, and level shifting to ensure compatibility with the analog-to-digital converter (ADC). The ADC then converts the analog signals into digital data, which is read by a microcontroller unit (MCU). The MCU performs initial processing and transmits the data to a computer (PC) for storage, visualization, or further analysis (e.g., AI processing).

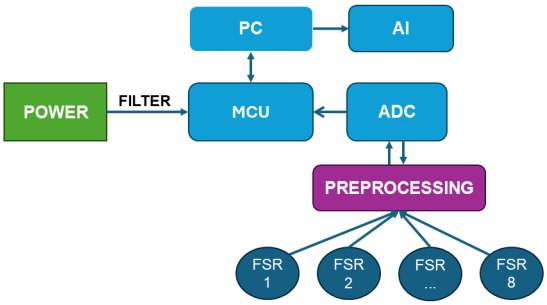

Fig. 3. Block diagram of the sensor data acquisition system.

Given the small variations in sensor resistance and the need for a sufficiently high sampling rate to capture dynamic human movements, the STM32F103C8T6 micro-controller was selected due to its 72 MHz clock speed. In addition, the system incorporates the ADS1115 module, which offers a resolution of approximately 800 ADC counts within a 0.1V input range. To meet real-time measurement requirements and maintain high sampling frequency, the authors integrated the FreeRTOS (Real-Time Operating System) into the system.

FreeRTOS enables concurrent (logically parallel) execution of tasks such as sensor data reading and data transmission. This design optimizes system performance and minimizes data loss when the MCU is occupied with processing or communication tasks.

C. Compressed sensing method – Data reconstruction

1) Compressed sensing model for plantar pressure map reconstruction: Compressed sensing (CS) is a signal acquisition and reconstruction framework that enables accurate recovery of high-dimensional signals from a significantly reduced number of measurements by exploiting sparsity in an appropriate representation domain. This paradigm is particularly well suited to plantar-pressure measurement systems, where the number of available physical sensors is inherently limited.

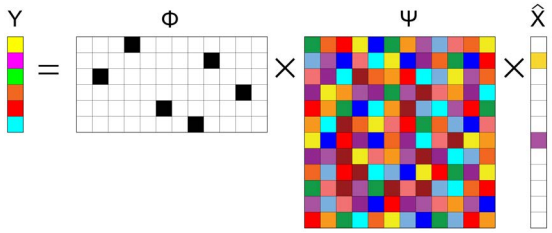

Fig. 4. Schematic of measurements in the compressed sensing framework [11].

Within the CS framework, the plantar pressure distribution $X \in \mathbb{R}^N$ is not directly observed. Instead, a reduced set of linear measurements is acquired through a sensing matrix $\Phi \in \mathbb{R}^{M\times N}$, with $M \ll N$, according to:

$$Y = \Phi X \tag{3}$$

When the pressure map admits a sparse representation in a dictionary Ψ, i.e., $X = \Psi\hat{X}$, the measurement model can be equivalently expressed as:

$$Y = \Phi\Psi\hat{X} \tag{4}$$

Reconstruction of the full plantar pressure map is then formulated as a sparse recovery problem, in which the objective is to estimate the sparse coefficient vector $\hat{X}$ from the compressed measurements Y. Fig. 4 illustrates the schematic of the measurement process in the compressed sensing framework, highlighting the relationship between the original pressure map, the sensing matrix, and the compressed measurements. In the considered plantar-pressure application, measurements are obtained via single-point pressure sensors, and the sensing matrix Φ is therefore fixed and directly determined by the physical sensor layout. By exploiting a learned dictionary Ψ and sparse recovery algorithms, the full plantar pressure distribution can be reconstructed from these limited sensor measurements.

2) Dictionary Learning and Sparse Recovery Algorithms (K-SVD and OMP): To enable sparse representations of plantar pressure maps within the compressed sensing framework, a data-driven dictionary is first learned using the K-SVD algorithm. K-SVD is an iterative dictionary learning algorithm that seeks an overcomplete dictionary Ψ enabling each training sample x_i to admit a sparse representation $\hat{x}_i$ such that $x_i \approx \Psi\hat{x}_i$:

$$\min_{\Psi,\{\hat{x}_i\}} \sum_{i=1}^{N} \|x_i - \Psi\hat{x}_i\|_2^2 \quad \text{s.t.} \quad \|\hat{x}_i\|_0 \le s, \tag{5}$$

where s denotes the prescribed sparsity level. This objective constitutes the loss function minimized during training. The algorithm alternates between two stages. In the sparse-coding stage, the dictionary Ψ is fixed and each sparse vector $\hat{x}_i$ is estimated by solving equation (6), typically using Orthogonal Matching Pursuit (OMP).

$$\hat{x}_i = \arg\min_{\hat{x}} \|x_i - \Psi\hat{x}\|_2^2 \quad \text{s.t.} \quad \|\hat{x}\|_0 \le s \tag{6}$$

In the dictionary-update stage, each atom ψ_k is refined by isolating its contribution to the representation error. Let E_k (equation(7)) be the residual matrix excluding atom k, and let $E_k^{(R)}$ contain only the columns for which the coefficient associated with ψ_k is nonzero.

$$E_k = X - \sum_{j\neq k} \psi_j \hat{x}_j^\top \tag{7}$$

Applying singular value decomposition $E_k^{(R)} = U\Sigma V^\top$, the atom and its active coefficients are jointly updated as $\psi_k = U(:,1); \hat{x}_k^{(R)} = \Sigma(1,1)V(:,1)$. Through this alternating procedure, K-SVD progressively refines both dictionary atoms and sparse codes to achieve increasingly accurate sparse representations of the training data.

Given the learned dictionary, sparse coefficient estimation from compressed measurements is then performed using Orthogonal Matching Pursuit (OMP). Orthogonal Matching Pursuit (OMP) is a greedy sparse-recovery algorithm used to estimate a sparse representation $\hat{x}$ from compressed measurements. In the compressed sensing model $y = \Phi x = \Phi\Psi\hat{x}$, OMP seeks the sparse vector $\hat{x}$ whose dictionary-based synthesis $\Psi\hat{x}$ best matches the measurements. At each iteration, the algorithm identifies the dictionary atom that has the highest correlation with the current residual, augments the active set of selected atoms, and solves a constrained least-squares problem to update the estimate of $\hat{x}$. The residual is then recomputed and the process repeats until a predefined sparsity level or reconstruction criterion is satisfied. Thus, OMP provides the sparse coefficients required to reconstruct the foot-pressure signal under limited sensing.

3) Experimental Model Construction: Fig. 1 illustrates the eight sensor positions as pixels in the image. These positions directly determine the structure of the sensing matrix Φ. After determining the sensor locations, the pressure map X is flattened by stacking the columns of the original pressure image (with resolution $n_1 \times n_2 = 40 \times 20$) into a single vector of 800 length. The matrix Φ serves to select the corresponding values from X to form the measurement vector P.

Specifically, Φ is a binary matrix of size $M \times N$, where each row contains a single value of 1 at the index corresponding to the position of a sensor in the flattened vector X. The non-zero elements of matrix Φ are visualized in **Table I**.

Finally, to reconstruct the original signal, a basis matrix Ψ of size $N \times N'$ is required. In this study, the authors selected $N' = 50$, resulting in a transform basis matrix Ψ of size 800×50. Training this matrix Ψ so that the transformed signal $\hat{X}$ is sufficiently sparse helps to improve the accuracy of reconstruction. In the experiments, a sparsity level of $s = 2$ was chosen.

TABLE I
SENSOR POSITION MAPPING IN MATRIX Φ

Index	Value	
284	7.0	(0, 352, 1)
290	6.0	(1, 540, 1)
340	3.0	(2, 340, 1)
352	1.0	(3, 535, 1)
446	8.0	(4, 451, 1)
451	5.0	(5, 290, 1)
535	4.0	(6, 284, 1)
540	2.0	(7, 446, 1)

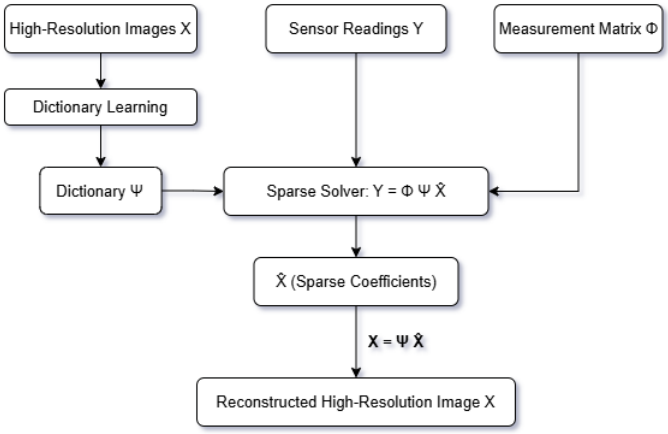

Fig. 5. Diagram of Dictionary Learning and Image Reconstruction.

The input data used in this study was sourced from a publicly available "*Pressure Sensor Heatmap-RGB*" dataset on `Kaggle.com` [12], a well-known platform that provides machine learning datasets and model examples. This data set comprises 1801 images of plantar pressure heat maps, each 224 x 224, from both feet, and was originally designed for applications in gait analysis and anomaly detection in medical diagnostics. Based on the data set, the authors reconstructed the plantar pressure maps following the procedure illustrated in Fig. 5.

III. RESULTS

A. Sensor Calibration Results

To calibrate the sensors, different standard weights were applied to generate the corresponding resistance values. These resistance changes, in turn, caused variations in the output voltage of the voltage divider circuit. For this reason, the authors chose to use ADC values to plot the relationship between pressure and resistance. The corresponding figure shows that the sensor error ranges from 0% to 5%, depending both on the sensor characteristics and on the measurement systems itself. The fitted equations in the plot follow an exponential function form. The coefficient of determination $\mathbb{R}^2$, which measures how well a regression model explains the variation in the predicted data compared to the actual data, was used to assess the quality of the fit (Fig. 6). It is calculated as follows:

$$R^2 = 1 - \frac{SS_{\text{res}}}{SS_{\text{tot}}} \tag{8}$$

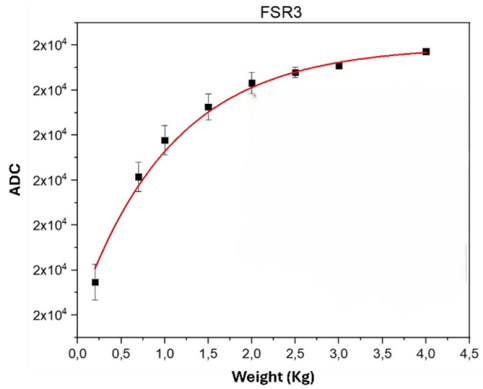

Fig. 6. Graph of the relationship between pressure and ADC.

where SS_{res} is the residual sum of squares between the actual and predicted values, and SS_{tot} is the total sum of squares between the actual values and their mean.

The value R^2 represents the reliability of the fitted model in capturing the data trend. In this study, the R^2 values for the pressure-ADC relationship reached 0.98, indicating that the curve can closely approximate the actual pressure values based on the ADC readings.

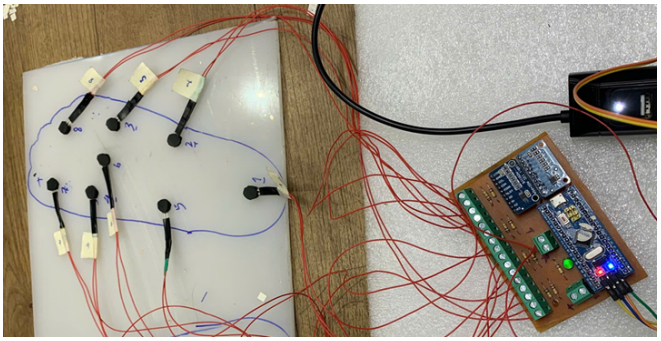

Fig. 7. Experimental plantar pressure measurement array.

The derived equations serve as the foundation for the construction of the foot pressure measurement system, which includes eight sensors. Each sensor requires a separate calibration equation to predict the pressure values from the ADC readings. This approach helps minimize potential errors in the measurement system by accounting for the individual characteristics and variability of each sensor.

B. Plantar Pressure Measurement System

A healthy volunteer with no known foot disorders and a body weight of 65 kg applied static pressure to the measurement system, where the pressure sensors were arranged as shown in Fig. 7.

The signals acquired from the sensors were passed through calibration functions specific to each sensor, as shown in Table II.

From Table II, it is evident that sensors located at positions 1, 3, 4 and 7 recorded significantly higher values compared to the others. This reflects the non-uniform pressure distribution under the plantar surface. These sensor positions correspond to anatomical regions such as the heel, metatarsal heads, and the area near the big toe – which are typically the main load bearing regions during standing. In contrast, the sensor at position 5 consistently recorded near-zero values throughout all measurements, indicating a region not in direct contact with the surface-consistent with the anatomical location of the medial arch. Other sensors, such as those at positions 2, 6, and 8, reported low pressure values, suggesting they are located in areas that bear minimal load.

TABLE II
CALIBRATED PRESSURE VALUES AT EACH SENSOR POSITION

STT	ST1	ST2	ST3	ST4	ST5	ST6	ST7	ST8
1	3.65	0.27	1.03	0.90	0.00	0.17	2.36	0.07
2	4.43	0.27	0.98	0.80	0.00	0.17	2.52	0.08
3	4.01	0.28	1.30	1.10	0.00	0.20	1.81	0.06
4	4.05	0.32	1.22	1.10	0.00	0.21	2.17	0.07
5	4.48	0.35	1.42	1.10	0.00	0.12	1.63	0.06

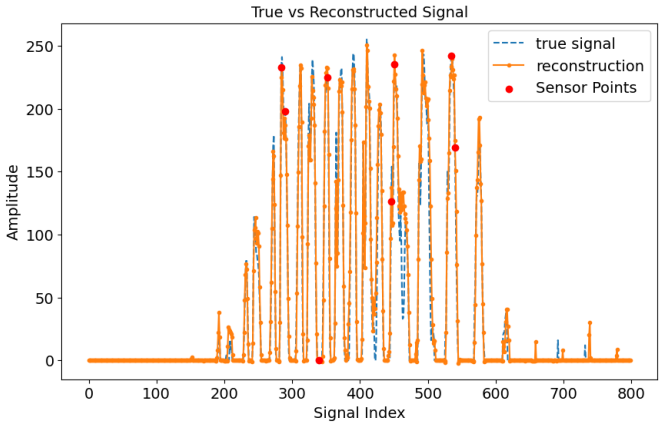

Fig. 8. Comparison between reconstructed and ground truth signal.

These findings indicate that the input signal naturally exhibits sparsity, with only a few positions registering significant pressure values. This sparsity is advantageous for applying compressed sensing methods. The calibrated data are then used to construct the measurement vector Y, and the sparse spatial structure of the signal improves the reconstruction performance when using OMP algorithms.

C. Training AI Using the Compressed Sensing (CS) Algorithm

After constructing all the necessary matrices for reconstructing the signal $\hat{X}$ from the measurement vector Y, the original signal X is estimated using the equation 5.

The input pressure map dataset was split into two subsets: 70% for training the K-SVD algorithm and the remaining 30% for testing purposes. A random image from the test set was selected to evaluate the reconstruction performance.

To verify the theoretical feasibility of sparse recovery, we evaluate the mutual incoherence between the sensing matrix Φ and the learned dictionary Ψ. Based on the standard definition of mutual incoherence

$$\mu = \max_{i,j} |\langle \phi_i, \psi_j \rangle|,$$

where all sensing vectors ϕ_i (rows of Φ) and basis atoms ψ_j (columns of Ψ) are normalized in the ℓ_2 sense, we obtain an incoherence value of approximately $\mu \approx 0.21$. According to the classical sufficient condition established by Donoho and Elad [13], and later refined in Tropp [14], accurate recovery of any s-sparse signal via ℓ_1 minimization is guaranteed whenever:

$$s < \frac{1}{2}\left(1 + \frac{1}{\mu}\right) \tag{9}$$

Substituting $\mu = 0.21$ yields, $s < 2.88$, indicating that theoretical guarantees hold only for signals with sparsity level up to $s = 2$.

In the context of plantar-pressure measurement with a severely limited number of sensors, the acquisition process must rely on single-point measurements, leading to a Single-Pixel sensing matrix. An incoherence level of $\mu \approx 0.21$ suggests a moderate degree of incompatibility between Φ and Ψ, which may be acceptable for signals with very low intrinsic sparsity.

Fig. 8 clearly demonstrates the resemblance between the original and reconstructed signals when represented as one-dimensional vectors. Fig. 9 compares the original and reconstructed pressure maps after reshaping them back into two-dimensional space. Despite using only data from 8 sensors, the reconstruction algorithm successfully preserves the shape and spatial characteristics of the original image. This demonstrates the feasibility of reconstructing plantar pressure maps using the Compressed Sensing (CS) approach, especially in applications with a limited number of sensors.

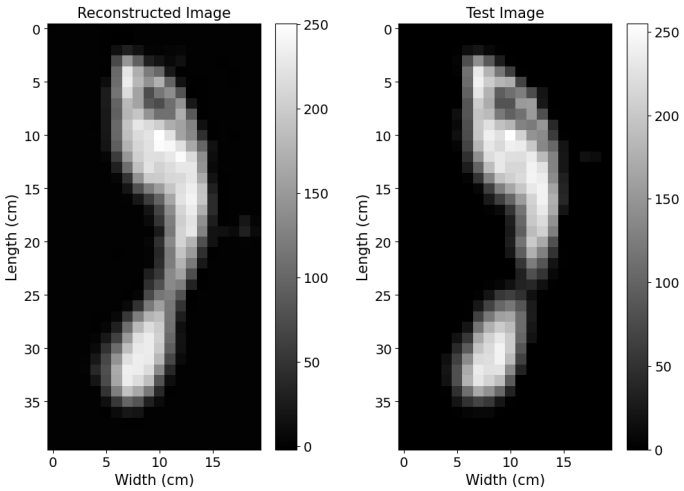

Fig. 9. Ground Truth and Reconstructed Pressure Maps.

To quantify the similarity between the original and reconstructed images, the Pearson correlation coefficient was employed, calculated as follows:

$$r = \frac{\sum(x_i - \bar{x})(y_i - \bar{y})}{\sqrt{\sum(x_i - \bar{x})^2}\sqrt{\sum(y_i - \bar{y})^2}} \tag{10}$$

To evaluate the Pearson correlation of the algorithm, the authors only considered values above 5 in Fig. 8, as points close to zero correspond to locations without applied force.

The results show a Pearson correlation of 97.43% in Fig. 8 and an average Pearson coefficient of 95.01% across the test set.

D. Reconstruction of Plantar Pressure Maps Using Compressive Sensing

Based on experimental data collected from the pressure measurement system with 8 sensors, the authors carried out the reconstruction of plantar pressure distribution images using a pre-trained model. Since the images in the initial training set were normalized with a maximum pixel value of approximately 255, the actual measured values from the sensor were adjusted to ensure consistency in the value domain. Specifically, the authors scaled the measured sensor values by an appropriate factor to align them with the range of the training data.

Fig. 10 illustrates the result of reconstructing a plantar pressure image from 8 input values corresponding to the positions of the sensors. The reconstructed image demonstrated the algorithm's ability to recover the overall shape of the plantar pressure distribution, including key structural features such as pressure points under the heel and toes. Despite the limited number of input sensors, the employed Compressed Sensing algorithm successfully reconstructed an image with high structural similarity to the training data in terms of both shape and pixel distribution.

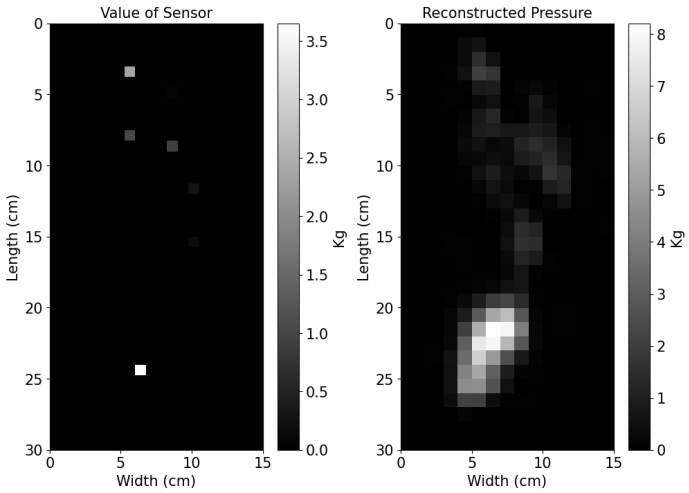

Fig. 10. Reconstruction from 8 sensor values using the CS algorithm.

IV. CONCLUSION

Upon completing the proposed tasks, the authors developed a standardized resistive sensor system, establishing individual calibration equations for each sensor integrated into the generalized 8-sensor pressure measurement framework. This system, combined with the Compressed Sensing (CS) algorithm, enabled the reconstruction of plantar pressure maps from limited sensor input.

In the future, this work can be extended by deploying FSR sensors on larger mats that cover the full contact area of the foot during gait. Increasing both the sensor density and distribution area would improve spatial resolution and enable more comprehensive data acquisition, especially for analyzing complex or abnormal gait patterns, such as those observed in individuals with disabilities.

Furthermore, instead of relying solely on simulated or normalized data, the system could integrate AI training processes using actual measurements from a diverse group of participants. This approach would enable the model to learn the natural variations in gait and pressure distribution across different walking patterns, thereby enhancing the accuracy and adaptability of the reconstructed pressure maps.

Finally, incorporating deep learning techniques and real-time processing could unlock broader applications in continuous motion tracking systems, personalized rehabilitation support, and early detection of gait anomalies.

ACKNOWLEDGMENT

This research was financially supported by the Ministry of Education and Training of Vietnam under Project B2025-BKA-07. The authors also acknowledge the AViS Lab at the Posts and Telecommunications Institute of Technology (PTIT) for its valuable support in the completion of this work.

REFERENCES

[1] M. J. Domínguez-Morales, F. Luna-Perejón, L. Miró-Amarante, M. Hernández-Velázquez, and J. L. Sevillano-Ramos, "Smart footwear insole for recognition of foot pronation and supination using neural networks," *Applied Sciences (Switzerland)*, vol. 9, no. 19, 2019.

[2] Y. Dai, J. Gao, W. Zhang, X. Wu, X. Zhu, and W. Gu, "Smart insoles for gait analysis based on meshless conductive rubber sensors and neural networks," *Journal of Physics: Conference Series*, vol. 2500, no. 1, 2023.

[3] V. Bucinskas, A. Dzedzickis, J. Rozene, and J. Subaciute-zemaitiene, "Wearable feet pressure sensor for human gait and falling diagnosis," 2021.

[4] A. Fatema, S. Poondla, R. B. Mishra, and A. M. Hussain, "A low-cost pressure sensor matrix for activity monitoring in stroke patients using artificial intelligence," *IEEE Sensors Journal*, vol. 21, no. 7, pp. 9546–9552, 2021.

[5] A. H. A. Razak, A. Zayegh, R. K. Begg, and Y. Wahab, "Foot plantar pressure measurement system: A review," *Sensors (Switzerland)*, vol. 12, no. 7, pp. 9884–9912, 2012.

[6] J. Park *et al.*, "Foot plantar pressure measurement system using highly sensitive crack-based sensor," *Sensors (Switzerland)*, vol. 19, no. 24, pp. 1–10, 2019.

[7] T. Keatsamarn, S. Visitsattapongse, C. Pintavirooj, and H. Aoyama, "Optical-based foot plantar pressure measurement with application in human postural balance, gait and recognition analysis," in *Proceedings of the 2020 6th International Conference on Engineering, Applied Sciences and Technology (ICEAST)*, pp. 8–11, 2020.

[8] I. Technologies, "Fsr 402 data sheet," 2013. [Online]. Available: http://www.interlinkelectronics.com/FSR402short.php.

[9] L. Paredes-Madrid, C. A. Palacio, A. Matute, and C. A. P. Vargas, "Underlying physics of conductive polymer composites and force sensing resistors (fsrs) under static loading conditions," *Sensors (Switzerland)*, vol. 17, Sept. 2017.

[10] M. Milovic, G. Farías, D. Yunge, S. Fingerhuth, F. Pizarro, and G. Hermosilla, "Detection of human gait phases using textile pressure sensors: A low cost and pervasive approach," *Sensors (Switzerland)*, vol. 22, no. 8, 2022.

[11] L. C. Ludeman, *Fundamentals of Digital Signal Processing*. Wiley, 1991.

[12] A. Goldbloom, "Kaggle." [Online]. Available: https://www.kaggle.com/.

[13] D. L. Donoho and M. Elad, "Optimally sparse representation in general (nonorthogonal) dictionaries via ℓ_1 minimization," *Proceedings of the National Academy of Sciences*, vol. 100, pp. 2197–2202, Mar. 2003.

[14] J. Tropp, "Greed is good: algorithmic results for sparse approximation," *IEEE Transactions on Information Theory*, vol. 50, no. 10, pp. 2231–2242, 2004.